

Elliptical phantoms for tomographic reconstruction

—
Sub-pixel image processing

Tom Szwagier ^{1,2}

¹ENS Paris-Saclay, Gif-sur-Yvette, France

²Mines Paris, Paris, France

April 26th, 2022



Table of content

1 Introduction

- Motivations
- Related works
- Contributions

2 Prerequisites on Computed Tomography reconstruction

3 Continuous reconstruction

- Fourier Transform
- Radon Transform
- Fourier slice theorem

4 Discrete reconstruction

- Discrete Fourier Transform of the discrete Radon Transform
- Interpolation of the radial Discrete Fourier Transform
- Inverse Fourier Transform of the interpolated Fourier spectrum

5 Inverse Crime

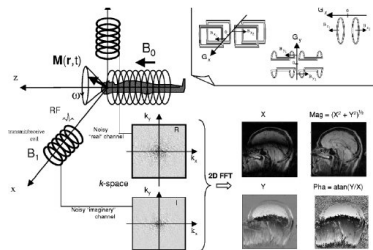
6 Results on more complex phantoms

- Tiny rotated and translated ellipse
- Complex phantom as a combination of ellipses

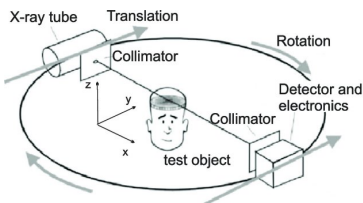
7 Conclusion

Medical images are acquired through the measurement of biological quantities:

- **MRI:** distribution of proton spin density (**Brown et al. 2014**)
- **CT-scan:** distribution of X-ray attenuation coefficients (**Herman 2009**)



(a) Principles of MRI acquisition
(Lysaker, Lundervold, and Tai 2003)



(b) Principle of computed tomography
(Bauer, Chaves, and Arcoumanis 2012)

Inverse problem:

- **MRI:** discrete K-space measurements → Total Variation reconstruction
(Rudin, Osher, and Fatemi 1992) (Abergel and Moisan 2017)
- **CT-scan:** discrete Radon measurements → incomplete frequency space

Analysis of the reconstruction:

- the acquisition parameters have an impact on the quality of the reconstruction
- good reconstruction is primordial for medical diagnosis
- → simulations on *phantoms* (physical and numerical)

Inverse crime:

- when the same object is used both for simulation and reconstruction
- rasterized image might suffer from aliasing, yielding uninituitively overly optimistic results
- → search for analytical formulas on continuous phantoms

Analytical phantoms

(Larry A. Shepp and Logan 1974)

- ellipse-based phantom with 11 ellipses
- study the impact of the parameters on the reconstruction, from a general theoretical point of view
- apply it to a single regular ellipse

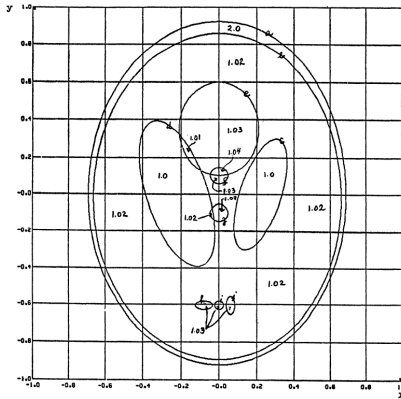
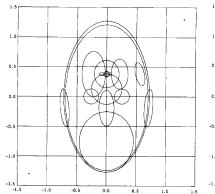


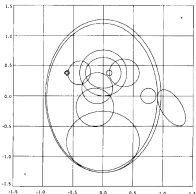
Figure: Shepp & Logan's phantom (Larry A. Shepp and Logan 1974)

(L. Shepp et al. 1980)

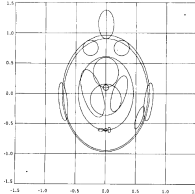
- 3D phantom with 17 ellipses
- provide their exact coordinates for reproducibility
- applications to NMR Computerized Tomography



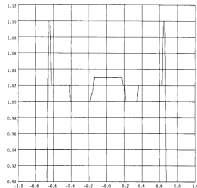
(a) Front view



(b) Side view



(c) Top view



(d) Projection along
the line
 $y = 0.23, z = 0.381$

Figure: Improved Shepp & Logan's phantom (L. Shepp et al. 1980)

(Koay, Sarlls, and Özarslan 2007)

- 3D phantom with more intuitive coordinates
- analytical formula for the Fourier coefficients
- sinusoidal and polynomial functions only, using advanced formulas from spherical wave functions theory
- application to 3D MRI reconstruction with the true Fourier coefficients

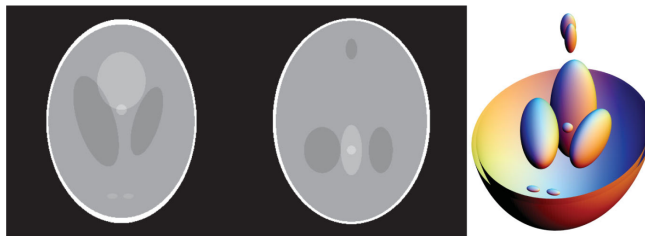


Figure: Visualization of several slices of (Koay, Sarlls, and Özarslan 2007)'s phantom as well as a 3D rendering

(Guerquin-Kern et al. 2012)

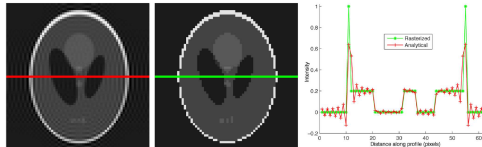
- more complex 2D model
- ellipses and piecewise-polynomial boundaries (spline, Bézier contours and polygons)
- closed-form Fourier Transform
- taking into account the MRI receiving-coil sensitivities (\rightarrow parallel MRI experiments, cf. **(Pruessmann et al. 1999)**)
- application to MRI reconstruction with true Fourier coefficients



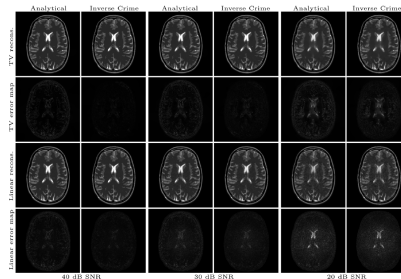
Figure: Illustration of (Guerquin-Kern et al. 2012)'s phantoms under study.
From Left to right: rectangle, ellipse and proposed one.

(Guerquin-Kern et al. 2012)

- put in perspective the *inverse crime* situation in medical image acquisition
- show how aliasing renders better in the inverse crime setting



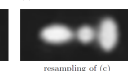
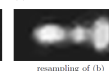
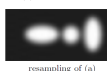
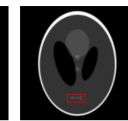
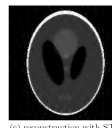
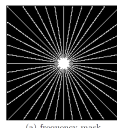
(a) Shepp & Logan's phantom reconstruction (*left*: analytical; *right*: inverse crime)



(b) Brain phantom reconstruction in the analytical vs. inverse crime setting

(Abergel and Moisan 2017)

- Shannon theory-based Total Variation (TV) reconstruction from sparse Fourier coefficients
- regularization based on the gradient of the Shannon interpolation of the image
- inverse crime situation when generating the k-space coefficients with DFT due to aliasing
- solved by generating a non-aliased version of the phantom by smoothing and downsampling



**(a) STV failing vs TV due to aliasing
(Abergel and Moisan 2017)**

(b) STV performing better than TV on the non-aliased version (Abergel and Moisan 2017)

Contributions

- homemade 2D ellipse-based phantom
- analytical formulas related to CT reconstruction and inverse crime
- implementation and analysis of the parameters' impact on the reconstruction

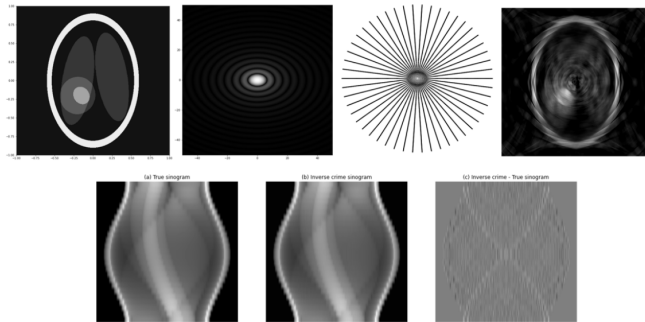


Figure: Illustrative summary of the contributions

Table of content

1 Introduction

- Motivations
- Related works
- Contributions

2 Prerequisites on Computed Tomography reconstruction

3 Continuous reconstruction

- Fourier Transform
- Radon Transform
- Fourier slice theorem

4 Discrete reconstruction

- Discrete Fourier Transform of the discrete Radon Transform
- Interpolation of the radial Discrete Fourier Transform
- Inverse Fourier Transform of the interpolated Fourier spectrum

5 Inverse Crime

6 Results on more complex phantoms

- Tiny rotated and translated ellipse
- Complex phantom as a combination of ellipses

7 Conclusion

Photoelectric effect

$$dI = -I(x)\rho(x)dx \Rightarrow I(x) = I_0 \exp\left(-\int_0^x \rho(t)dt\right)$$

$\rho(x)$: local X-ray attenuation coefficient.

Theorem (Fourier slice theorem (Kak and Slaney 2001))

The 1D Fourier transform of a parallel projection of an image $f(x, y)$ at an angle θ gives a slice of the two-dimensional transform $F(u, v)$, subtending an angle θ with the u -axis.

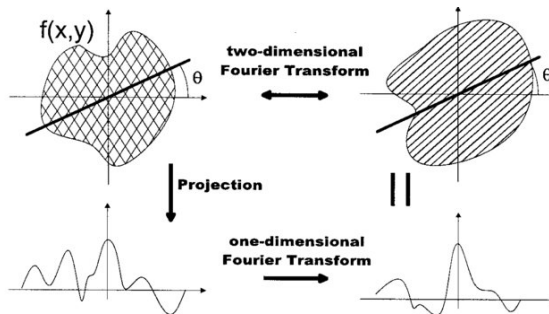


Figure: Illustration of the Fourier Slice Theorem (Ripoll, Kettunen, and Herzog 2002)

Line equation:

$$t = x \cos \theta + y \sin \theta \quad (1)$$

Radon transform at angle θ :

$$\mathcal{R}_\theta(t) = \int_{\theta, t \text{ line}} \rho(t, s) ds \quad (2)$$

Fourier Transform:

$$S_\theta(\omega) = \int_{-\infty}^{-\infty} \mathcal{R}_\theta(t) e^{-i\omega t} dt = \int_{-\infty}^{+\infty} \left[\int_{\theta, t \text{ line}} \rho(t, s) ds \right] e^{-i\omega t} dt \quad (3)$$

Can be re-written using (1) as:

$$S_\theta(\omega) = \int_{-\infty}^{+\infty} \int_{-\infty}^{+\infty} \rho(x, y) e^{-i\omega(x \cos \theta + y \sin \theta)} dx dy \quad (4)$$

Leads to the Fourier Slice Theorem:

$$S_\theta(\omega) = F(\omega \cos \theta, \omega \sin \theta) \quad (5)$$

→ the knowledge of all the (θ, t) projections makes possible by Inverse Fourier Theorem to recover the original continuous image.

Table of content

- 1 Introduction**
 - Motivations
 - Related works
 - Contributions
- 2 Prerequisites on Computed Tomography reconstruction**
- 3 Continuous reconstruction**
 - Fourier Transform
 - Radon Transform
 - Fourier slice theorem
- 4 Discrete reconstruction**
 - Discrete Fourier Transform of the discrete Radon Transform
 - Interpolation of the radial Discrete Fourier Transform
 - Inverse Fourier Transform of the interpolated Fourier spectrum
- 5 Inverse Crime**
- 6 Results on more complex phantoms**
 - Tiny rotated and translated ellipse
 - Complex phantom as a combination of ellipses
- 7 Conclusion**

Simple ellipse:

$$\rho_{(a,b)}(x, y) = \begin{cases} 1 & \text{if } \left(\frac{x}{a}\right)^2 + \left(\frac{y}{b}\right)^2 \leq 1 \\ 0 & \text{otherwise} \end{cases} \quad (6)$$

$$\hat{\rho}_{(a,b)}(k_x, k_y) = \int_{-\infty}^{+\infty} \int_{-\infty}^{+\infty} \rho_{(a,b)}(x, y) e^{-i(k_x x + k_y y)} dx dy \quad (7)$$

$$= \int_{\left(\frac{x}{a}\right)^2 + \left(\frac{y}{b}\right)^2 \leq 1} e^{-i(k_x x + k_y y)} dx dy \quad (8)$$

$$\left(X = \frac{x}{a}; Y = \frac{y}{b} \right) \quad (9)$$

$$= \int_{X^2 + Y^2 \leq 1} e^{-i(k_x a X + k_y b Y)} ab dX dY \quad (10)$$

$$(X = r \cos(\theta); Y = r \sin(\theta)) \quad (11)$$

$$= ab \int_{r=0}^1 r \left[\int_{\theta=0}^{2\pi} e^{-i(k_x a r \cos(\theta) + k_y b r \sin(\theta))} d\theta \right] dr \quad (12)$$

$$\int_{\theta=0}^{2\pi} e^{-ic \cos(\theta+\varphi)} d\theta = 2\pi J_0(-c) \quad (13)$$

- $c = \text{sgn}(k_x ar) \sqrt{(k_x ar)^2 + (k_y br)^2} = \text{sgn}(k_x) \sqrt{(k_x a)^2 + (k_y b)^2} r$
- J_0 : Bessel function of the first kind of order $\alpha = 0$

$$\hat{\rho}_{(a,b)}(k_x, k_y) = ab \int_{r=0}^1 r \left[\int_{\theta=0}^{2\pi} e^{-i(k_x ar \cos(\theta) + k_y br \sin(\theta))} d\theta \right] dr \quad (14)$$

$$= ab \int_{r=0}^1 r [2\pi J_0(-c)] dr \quad (15)$$

$$\hat{\rho}_{(a,b)}(k_x, k_y) = 2\pi ab - \frac{J_1 \left(\sqrt{(k_x a)^2 + (k_y b)^2} \right)}{\sqrt{(k_x a)^2 + (k_y b)^2}} \quad (16)$$

More complex ellipse

$\mathcal{E}(a, b, \theta, r_0)$ ellipse of axes (a, b) , center $r_0 = (x_0, y_0)$ with a previous rotation of angle θ .

Mapping: $r \rightarrow R(\theta)^T(r - r_0)$, with $R(\theta) = \begin{pmatrix} \cos(\theta) & -\sin(\theta) \\ \sin(\theta) & \cos(\theta) \end{pmatrix}$.

$$\hat{\rho}_{(a,b,\theta,r_0)}(k) = \int_{r \in \mathcal{E}_{(a,b,\theta,r_0)}} e^{-ir \cdot k} dr \quad (17)$$

$$= \int_{u \in \mathcal{E}_{(a,b)}} e^{-i(r_0 + R(\theta)u) \cdot k} du \quad (18)$$

$$(r = r_0 + R(\theta)u) \quad (19)$$

$$= e^{-ir_0 \cdot k} \int_{u \in \mathcal{E}_{(a,b)}} e^{-i(R(\theta)u) \cdot k} du \quad (20)$$

$$= e^{-ir_0 \cdot k} \int_{u \in \mathcal{E}_{(a,b)}} e^{-iu \cdot (R(\theta)^\top k)} du \quad (21)$$

$$= e^{-ir_0 \cdot k} \hat{\rho}_{(a,b)}(R(\theta)^\top k) \quad (22)$$

$$= e^{-ir_0 \cdot k} |\text{diag}(a, b)| \left(2\pi \frac{J_1(\|\text{diag}(a, b)(R(\theta)^\top k)\|_2)}{(\|\text{diag}(a, b)(R(\theta)^\top k)\|_2)} \right) \quad (23)$$

$$\hat{\rho}_{(a,b,\theta,r_0)}(k) = 2\pi ab \cdot e^{-ir_0 \cdot k} \frac{J_1(\|\text{diag}(a, b)R(\theta)^\top k\|_2)}{(\|\text{diag}(a, b)R(\theta)^\top k\|_2)} \quad (24)$$

Comments on the FT formula:

- non-compact support of Bessel functions → high-frequency components (expected from the ellipse-background discontinuity)
- affine scaling by $\text{diag}(a, b)$ → elliptical Airy pattern with inverted axes with respect to the original ellipse
- rotation of angle θ → rotation with the same angle of the ellipse in the Fourier domain
- translation makes the up-to-now real Fourier Transform become complex, introducing a non piecewise-constant phase

Remarks:

- Fourier transform of a disk had actually been implicitly tackled in the course (Fraunhofer Diffraction)
- but enabled me to manipulate Bessel properties which would turn out to be useful later

Line equation:

$$x \cos \theta + y \sin \theta = t \quad (25)$$

Re-parameterized as:

$$\begin{cases} x = t \cos \theta - z \sin \theta \\ y = t \sin \theta + z \cos \theta \end{cases} \quad (26)$$

$$\mathcal{R}_\theta(t) = \int_{-\infty}^{+\infty} \rho(t \cos \theta - z \sin \theta, t \sin \theta + z \cos \theta) dz \quad (27)$$

$$= \int_{-\infty}^{+\infty} \mathbb{1}_{\{x(z), y(z)\} \in \mathcal{E}(a, b)}(z) dz \quad (28)$$

$$= \int_{-\infty}^{+\infty} \mathbb{1}_{\left\{ \left(\frac{x(z)}{a}\right)^2 + \left(\frac{y(z)}{b}\right)^2 \leq 1 \right\}}(z) dz \quad (29)$$

$$= \int_{-\infty}^{+\infty} \mathbb{1}_{\left\{ \left(\frac{t \cos \theta - z \sin \theta}{a}\right)^2 + \left(\frac{t \sin \theta + z \cos \theta}{b}\right)^2 \leq 1 \right\}}(z) dz \quad (30)$$

Study the zeros of the polynomial:

$$P(z) = \left(\frac{t \cos \theta - z \sin \theta}{a} \right)^2 + \left(\frac{t \sin \theta + z \cos \theta}{b} \right)^2 - 1 \quad (31)$$

$$\Delta = 4 \frac{a^2 \cos^2 \theta + b^2 \sin^2 \theta - t^2}{a^2 b^2} \quad (32)$$

$$\boxed{\mathcal{R}_\theta(t) = 2ab \frac{\sqrt{a^2 \cos^2 \theta + b^2 \sin^2 \theta - t^2}}{a^2 \cos^2 \theta + b^2 \sin^2 \theta} \mathbb{1}_{\{t^2 \leq a^2 \cos^2 \theta + b^2 \sin^2 \theta\}}(t)} \quad (33)$$

Generalization to more complex ellipses using the following two basic properties:

- 1** *Rotation:* If $g(r, \theta) = f(r, \theta - \theta_0)$, then

$$\mathcal{R}^g_\theta(t) = \mathcal{R}^f_{\theta - \theta_0}(t) \quad (34)$$

- 2** *Translation:* If $g(x, y) = f(x - x_0, y - y_0)$, then

$$\mathcal{R}^g_\theta(t) = \mathcal{R}^f_\theta(t - x_0 \cos \theta - y_0 \sin \theta) \quad (35)$$

$$c := \sqrt{a^2 \cos^2 \theta + b^2 \sin^2 \theta} \quad (36)$$

$$\hat{\mathcal{R}}_\theta(\omega) = \frac{2ab}{c} \int_{-\infty}^{+\infty} \sqrt{c^2 - t^2} \mathbb{1}_{\{t^2 \leq c^2\}}(t) e^{-i\omega t} dt \quad (37)$$

$$= 4ab \int_0^1 \sqrt{1 - u^2} \cos(\omega cu) dt \quad (38)$$

$$= 4ab \int_0^{\frac{\pi}{2}} \sqrt{1 - \sin^2 \theta} \cos(\omega c \sin \theta) \cos \theta d\theta \quad (39)$$

$$(u = \sin \theta) \quad (40)$$

$$= 2ab \int_0^\pi \cos^2 \theta \cos(\omega c \sin \theta) d\theta \quad (41)$$

$$= ab\pi J_0(\omega c) + \frac{ab}{2}\pi (J_2(\omega c) + J_2(-\omega c)) \quad (42)$$

$$= ab\pi (J_0(\omega c) + J_2(\omega c)) \quad (43)$$

$$\hat{\mathcal{R}}_\theta(\omega) = 2\pi ab \frac{J_1(\omega c)}{\omega c} \quad (44)$$

$\hat{\mathcal{R}}_\theta(\omega) = \hat{\rho}_{(a,b)}(\omega \cos \theta, \omega \sin \theta)$

(45)

Table of content

- 1 Introduction**
 - Motivations
 - Related works
 - Contributions
- 2 Prerequisites on Computed Tomography reconstruction**
- 3 Continuous reconstruction**
 - Fourier Transform
 - Radon Transform
 - Fourier slice theorem
- 4 Discrete reconstruction**
 - Discrete Fourier Transform of the discrete Radon Transform
 - Interpolation of the radial Discrete Fourier Transform
 - Inverse Fourier Transform of the interpolated Fourier spectrum
- 5 Inverse Crime**
- 6 Results on more complex phantoms**
 - Tiny rotated and translated ellipse
 - Complex phantom as a combination of ellipses
- 7 Conclusion**

Real life:

- Finite number of sensors for parallel beams
- Finite number of angles
- → discrete approximation of the object

Choice of parameterization and notations:

$$\begin{cases} \forall n \in [0, N-1], \theta_n = \frac{n\pi}{N} \\ \forall k \in [0, S-1], t_k = -1 + \frac{2k}{S} \\ u : \Omega \rightarrow \mathbb{R}; \Omega = [0, N-1] \times [0, S-1] \end{cases} \quad (46)$$

Procedure

- 1 1D DFT on the discrete sinogram, angle by angle
- 2 Linear interpolation on the resulting discrete radial FT
- 3 Inverse FT on the interpolated Fourier spectrum

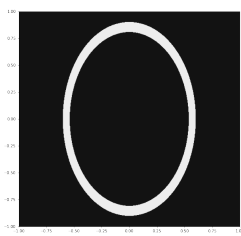
Reconstruction parameters¹:

$$\begin{cases} S &= 512 \\ N &= 25 \end{cases} \quad (47)$$

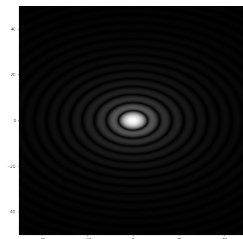
¹a typical couple of parameters is ($S = 512, N = 1000$), cf. *Upstate medical university – CT reconstruction*

Simple open uniform ellipse considered in the experiments:

$$\begin{cases} x_0 &= 0 \\ y_0 &= 0 \\ a_{ext} &= 0.6 \\ b_{ext} &= 0.9 \\ a_{int} &= 0.54 \\ b_{int} &= 0.81 \\ \theta &= 0 \end{cases} \quad (48)$$



(a) Uniform open ellipse



(b) Analytical FT (log scale)



(c) Analytical sinogram

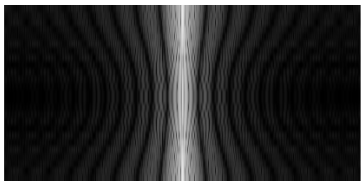
Figure: Illustration of the simple uniform elliptical phantom under study in this subsection, as well as its analytical Fourier Transform and sinogram

Discrete Fourier Transform of the discrete Radon Transform

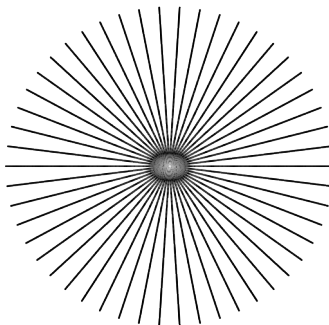
1D Discrete Fourier Transform at each angle θ_n :

$$\hat{u}_n(p) = \sum_{k=0}^{S-1} e^{-i\frac{2\pi p k}{S}} \mathcal{R}_{\frac{n\pi}{N}} \left(-1 + \frac{2k}{S} \right) \quad (49)$$

$$\hat{u}_n(p) = \frac{2ab}{a^2 \cos^2\left(\frac{n\pi}{N}\right) + b^2 \sin^2\left(\frac{n\pi}{N}\right)} \sum_{k=0}^{S-1} \sqrt{a^2 \cos^2\left(\frac{n\pi}{N}\right) + b^2 \sin^2\left(\frac{n\pi}{N}\right) - \left(-1 + \frac{2k}{S}\right)^2} e^{-i\frac{2\pi p k}{S}}$$



(a) DFT of the sinogram



(b) Cartesian visualization of the DFT

Figure: Illustration of the DFT of the discrete Radon Transform of the open ellipse

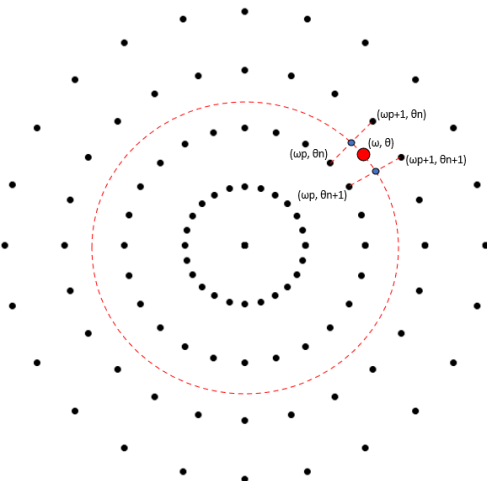


Figure: Schema of the radial Fourier Transform interpolation

Interpolation of the radial Discrete Fourier Transform

$$\hat{u}_{\text{interp}}(\omega \cos \theta, \omega \sin \theta) = \left(1 - \frac{\theta - \theta_n}{\theta_{n+1} - \theta_n}\right) \left[\left(1 - \frac{\omega - \omega_p}{\omega_{p+1} - \omega_p}\right) \hat{u}_n(p) + \left(\frac{\omega - \omega_p}{\omega_{p+1} - \omega_p}\right) \hat{u}_n(p+1) \right] + \left(\frac{\theta - \theta_n}{\theta_{n+1} - \theta_n}\right) \left[\left(1 - \frac{\omega - \omega_p}{\omega_{p+1} - \omega_p}\right) \hat{u}_{n+1}(p) + \left(\frac{\omega - \omega_p}{\omega_{p+1} - \omega_p}\right) \hat{u}_{n+1}(p+1) \right]$$
$$\omega \in [\omega_p, \omega_{p+1}[\iff \omega \in \left[-1 + \frac{2p}{S}, -1 + \frac{2(p+1)}{S}\right] \iff p = \left\lfloor \frac{(\omega+1)S}{2} \right\rfloor \implies \omega_p = -1 + \frac{2}{S} \left\lfloor \frac{(\omega+1)S}{2} \right\rfloor$$
$$\theta \in [\theta_n, \theta_{n+1}[\iff \theta \in \left[\frac{n\pi}{N}, \frac{(n+1)\pi}{N}\right] \iff n = \left\lfloor \frac{\theta N}{\pi} \right\rfloor \implies \theta_n = \frac{\left\lfloor \frac{\theta N}{\pi} \right\rfloor \pi}{N}$$
$$\hat{u}_{\text{interp}}(\omega \cos \theta, \omega \sin \theta) = \left(1 - \frac{\theta - \left\lfloor \frac{\theta N}{\pi} \right\rfloor \pi}{\frac{\theta N}{N}}\right) \left[\left(1 - \frac{\omega + 1 - \frac{2}{S} \left\lfloor \frac{(\omega+1)S}{2} \right\rfloor}{\frac{2}{S}}\right) \hat{u}_{\left\lfloor \frac{\theta N}{\pi} \right\rfloor} \left(\left\lfloor \frac{(\omega+1)S}{2} \right\rfloor\right) + \left(\frac{\omega + 1 - \frac{2}{S} \left\lfloor \frac{(\omega+1)S}{2} \right\rfloor}{\frac{2}{S}}\right) \hat{u}_{\left\lfloor \frac{\theta N}{\pi} \right\rfloor + 1} \left(\left\lfloor \frac{(\omega+1)S}{2} \right\rfloor + 1\right) \right]$$
$$+ \left(\theta - \frac{\left\lfloor \frac{\theta N}{\pi} \right\rfloor \pi}{N}\right) \left[\left(1 - \frac{\omega + 1 - \frac{2}{S} \left\lfloor \frac{(\omega+1)S}{2} \right\rfloor}{\frac{2}{S}}\right) \hat{u}_{\left\lfloor \frac{\theta N}{\pi} \right\rfloor + 1} \left(\left\lfloor \frac{(\omega+1)S}{2} \right\rfloor\right) + \left(\frac{\omega + 1 - \frac{2}{S} \left\lfloor \frac{(\omega+1)S}{2} \right\rfloor}{\frac{2}{S}}\right) \hat{u}_{\left\lfloor \frac{\theta N}{\pi} \right\rfloor + 1} \left(\left\lfloor \frac{(\omega+1)S}{2} \right\rfloor + 1\right) \right]$$

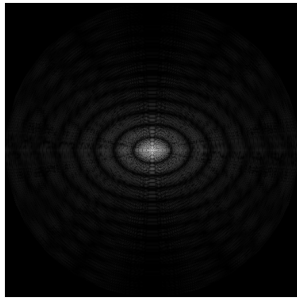


Figure: Interpolation of the radial Discrete Fourier Transform of the elliptical phantom's analytical sinogram

$$\begin{aligned}
 u(x, y) &= \int_{-\infty}^{+\infty} \int_{-\infty}^{+\infty} \hat{u}(k_x, k_y) e^{-i(k_x, k_y) \cdot (x, y)} dk_x dk_y \\
 &= \int_{-\infty}^{+\infty} \int_0^{\pi} \hat{u}(\omega \cos \theta, \omega \sin \theta) e^{-i\omega[x \cos \theta + y \sin \theta]} \omega d\omega d\theta
 \end{aligned}$$

$$\begin{aligned}
 u(x, y) &= \int_{-\infty}^{+\infty} \int_0^{\pi} e^{-i\omega[x \cos \theta + y \sin \theta]} \left(1 - \frac{\theta - \lfloor \frac{\theta N}{N} \rfloor \pi}{\frac{N}{S}} \right) \left[\left(1 - \frac{\omega + 1 - \frac{2}{S} \lfloor \frac{(\omega+1)S}{2} \rfloor}{\frac{S}{2}} \right) \hat{u}_{\lfloor \frac{\theta N}{\pi} \rfloor} \left(\lfloor \frac{(\omega+1)S}{2} \rfloor \right) + \left(\frac{\omega + 1 - \frac{2}{S} \lfloor \frac{(\omega+1)S}{2} \rfloor}{\frac{S}{2}} \right) \hat{u}_{\lfloor \frac{\theta N}{\pi} \rfloor} \left(\lfloor \frac{(\omega+1)S}{2} \rfloor + 1 \right) \right] \\
 &\quad + e^{-i\omega[x \cos \theta + y \sin \theta]} \left(\frac{\theta - \lfloor \frac{\theta N}{N} \rfloor \pi}{\frac{N}{S}} \right) \left[\left(1 - \frac{\omega + 1 - \frac{2}{S} \lfloor \frac{(\omega+1)S}{2} \rfloor}{\frac{S}{2}} \right) \hat{u}_{\lfloor \frac{\theta N}{\pi} \rfloor + 1} \left(\lfloor \frac{(\omega+1)S}{2} \rfloor \right) + \left(\frac{\omega + 1 - \frac{2}{S} \lfloor \frac{(\omega+1)S}{2} \rfloor}{\frac{S}{2}} \right) \hat{u}_{\lfloor \frac{\theta N}{\pi} \rfloor + 1} \left(\lfloor \frac{(\omega+1)S}{2} \rfloor + 1 \right) \right] \omega d\omega d\theta
 \end{aligned}$$

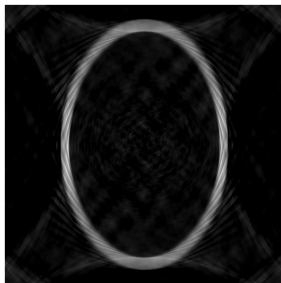
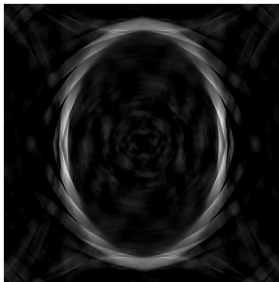
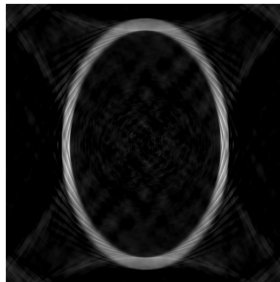


Figure: CT reconstruction of the open ellipse, with $N = 25$; $S = 512$

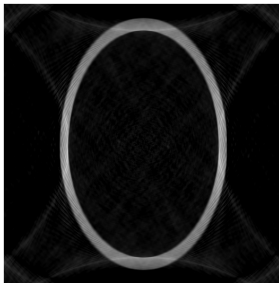
Reconstruction for several angular discretizations



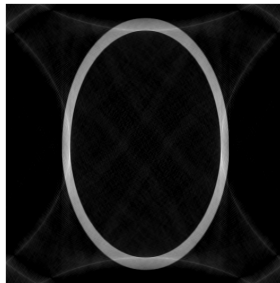
(a) $N=10$



(b) $N=25$



(c) $N=50$



(d) $N=100$

Table of content

1 Introduction

- Motivations
- Related works
- Contributions

2 Prerequisites on Computed Tomography reconstruction

3 Continuous reconstruction

- Fourier Transform
- Radon Transform
- Fourier slice theorem

4 Discrete reconstruction

- Discrete Fourier Transform of the discrete Radon Transform
- Interpolation of the radial Discrete Fourier Transform
- Inverse Fourier Transform of the interpolated Fourier spectrum

5 Inverse Crime

6 Results on more complex phantoms

- Tiny rotated and translated ellipse
- Complex phantom as a combination of ellipses

7 Conclusion

Discrete ellipse:

$$I^d(k, l) = \begin{cases} 1 & \text{if } \left(\frac{-1+\frac{2k}{L}}{a}\right)^2 + \left(\frac{-1+\frac{2l}{L}}{b}\right)^2 \leq 1 \\ 0 & \text{otherwise} \end{cases} \quad (50)$$

Interpolation:

$$I^c(x, y) = \left(1 - \frac{x-k}{\frac{L}{2}}\right) \left(1 - \frac{y-l}{\frac{L}{2}}\right) I^d(k, l) + \frac{x-k}{\frac{L}{2}} \left(1 - \frac{y-l}{\frac{L}{2}}\right) I^d(k+1, l) + \frac{y-l}{\frac{L}{2}} \left(1 - \frac{x-k}{\frac{L}{2}}\right) I^d(k, l+1) + \frac{x-k}{\frac{L}{2}} \frac{y-l}{\frac{L}{2}} I^d(k+1, l+1) \quad (51)$$

Rotation:

$$I^c \circ R(\theta)^{-1}(x, y) = I^c(x \cos \theta + y \sin \theta, -x \sin \theta + y \cos \theta) \quad (52)$$

Sampling:

$$I^d \circ R(\theta)^{-1}(k, l) = I^c \circ R(\theta)^{-1} \left(-1 + \frac{2k}{L}, -1 + \frac{2l}{L}\right) \quad (53)$$

Radon Transform:

$$\mathcal{R}_\theta(k) = \sum_{l=1}^L I^d \circ R(\theta)^{-1}(k, l) \quad (54)$$

$$\mathcal{R}_\theta(k) = \sum_{l=1}^L I^c \circ R(\theta)^{-1} \left(-1 + \frac{2k}{L}, -1 + \frac{2l}{L} \right) \quad (55)$$

$$\mathcal{R}_\theta(k) = \sum_{l=1}^L I^c \left(\left(-1 + \frac{2k}{L} \right) \cos \theta + \left(-1 + \frac{2l}{L} \right) \sin \theta, \left(1 - \frac{2k}{L} \right) \sin \theta + \left(-1 + \frac{2l}{L} \right) \cos \theta \right) \quad (56)$$

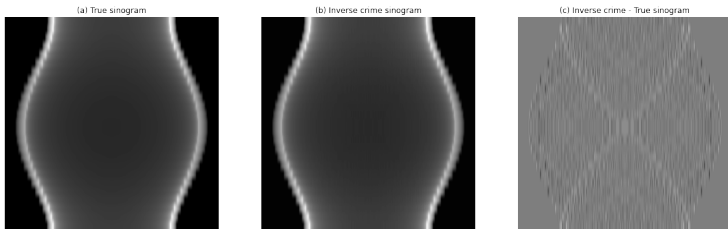
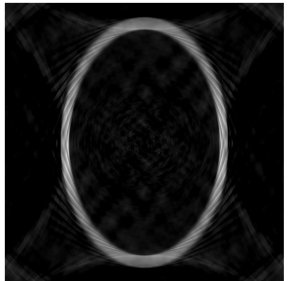
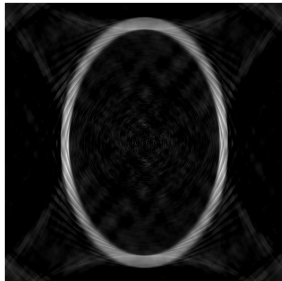


Figure: Comparison of the sinograms obtained with or without committing an inverse crime



(a) Reconstruction without inverse crime



(b) Reconstruction with inverse crime

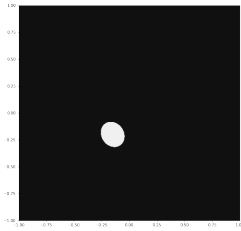
Figure: Comparison between the elliptical phantom reconstruction within the regular and inverse crime frameworks

Table of content

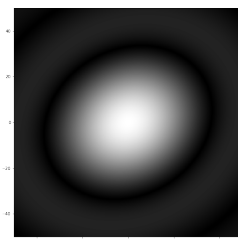
- 1 Introduction**
 - Motivations
 - Related works
 - Contributions
- 2 Prerequisites on Computed Tomography reconstruction**
- 3 Continuous reconstruction**
 - Fourier Transform
 - Radon Transform
 - Fourier slice theorem
- 4 Discrete reconstruction**
 - Discrete Fourier Transform of the discrete Radon Transform
 - Interpolation of the radial Discrete Fourier Transform
 - Inverse Fourier Transform of the interpolated Fourier spectrum
- 5 Inverse Crime**
- 6 Results on more complex phantoms**
 - Tiny rotated and translated ellipse
 - Complex phantom as a combination of ellipses
- 7 Conclusion**

Tiny rotated and translated ellipse

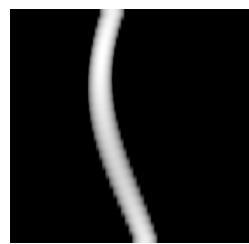
$$\begin{cases} x_0 &= -0.15 \\ y_0 &= -0.2 \\ a &= 0.1 \\ b &= 0.12 \\ \theta &= \frac{\pi}{6} \end{cases} \quad (57)$$



(a) Rotated and translated ellipse



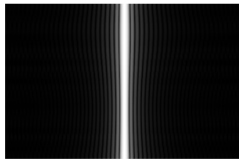
(b) Analytical FT (log scale)



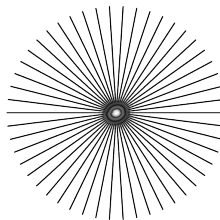
(c) Analytical sinogram

Figure: Illustration of the uniform rotated and translated elliptical phantom under study, as well as its analytical Fourier Transform and sinogram

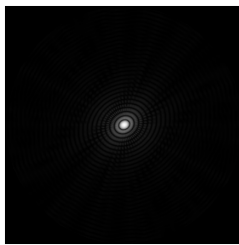
Tiny rotated and translated ellipse



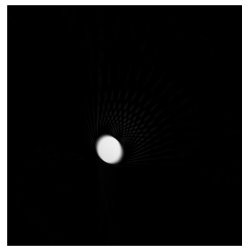
(a) Sinogram FT



(b) Sinogram FT radial



(c) Sinogram FT radial
interpolated



(d) Reconstruction

Figure: CT reconstruction of the uniform rotated and translated elliptical phantom under study

Tiny rotated and translated ellipse

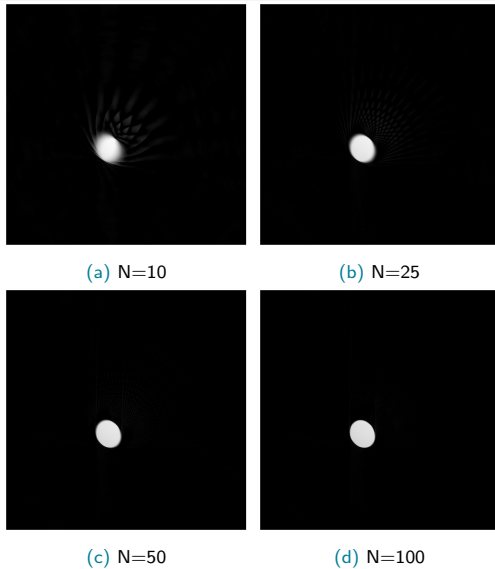


Figure: Impact of the angular discretization on the reconstruction

Tiny rotated and translated ellipse

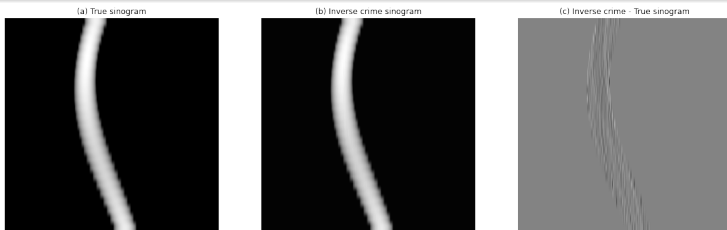
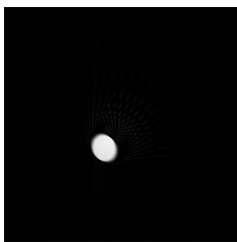
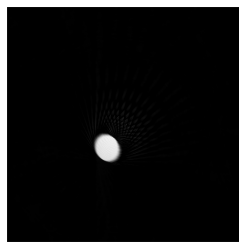


Figure: Comparison of the sinograms obtained with or without committing an inverse crime



(a) Reconstruction without inverse crime



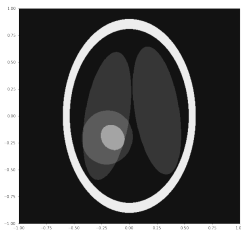
(b) Reconstruction with inverse crime

Figure: Comparison between the rotated and translated elliptical phantom reconstruction within the regular and inverse crime frameworks

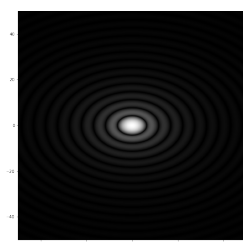
Complex phantom as a combination of ellipses

ρ	x_0	y_0	a	b	θ
5	0	0	0.6	0.9	0
-5	0	0	0.54	0.81	0
2	-0.15	-0.2	0.1	0.12	$\frac{\pi}{6}$
1	-0.2	-0.2	0.23	0.25	$-\frac{\pi}{20}$
1	-0.2	0	0.2	0.6	$-\frac{\pi}{20}$
1	0.25	0.05	0.2	0.6	$+\frac{\pi}{20}$

Table: Parameters for the full elliptical phantom



(a) Rotated and translated ellipse



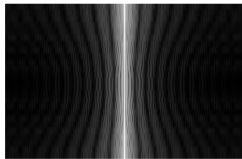
(b) Analytical FT (log scale)



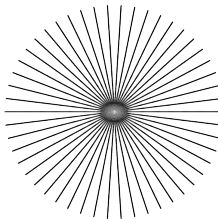
(c) Analytical sinogram

Figure: Illustration of the full phantom under study, as well as its analytical Fourier Transform and sinogram

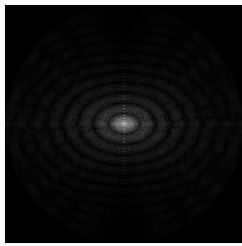
Complex phantom as a combination of ellipses



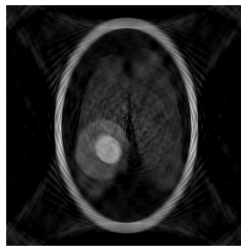
(a) Sinogram FT



(b) Sinogram FT radial



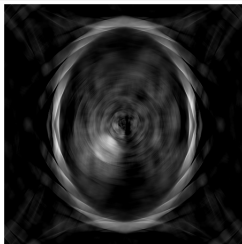
(c) Sinogram FT radial
interpolated



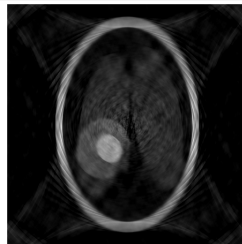
(d) Reconstruction

Figure: CT reconstruction of the full phantom under study

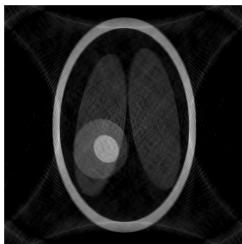
Complex phantom as a combination of ellipses



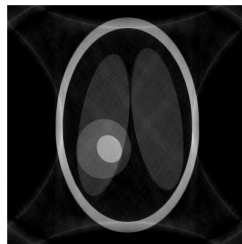
(a) $N=10$



(b) $N=25$



(c) $N=50$



(d) $N=100$

Figure: Impact of the angular discretization on the reconstruction

Complex phantom as a combination of ellipses

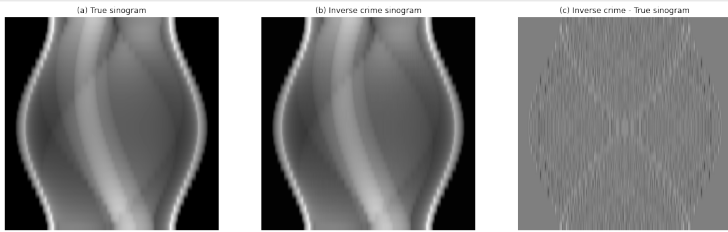


Figure: Comparison of the sinograms obtained with or without committing an inverse crime for the full phantom



(a) Reconstruction without inverse crime

(b) Reconstruction with inverse crime

Figure: Comparison between the full phantom reconstruction within the regular and inverse crime frameworks

Table of content

- 1** Introduction
 - Motivations
 - Related works
 - Contributions
- 2** Prerequisites on Computed Tomography reconstruction
- 3** Continuous reconstruction
 - Fourier Transform
 - Radon Transform
 - Fourier slice theorem
- 4** Discrete reconstruction
 - Discrete Fourier Transform of the discrete Radon Transform
 - Interpolation of the radial Discrete Fourier Transform
 - Inverse Fourier Transform of the interpolated Fourier spectrum
- 5** Inverse Crime
- 6** Results on more complex phantoms
 - Tiny rotated and translated ellipse
 - Complex phantom as a combination of ellipses
- 7** Conclusion

Contributions

- homemade 2D ellipse-based phantom
- analytical formulas related to CT reconstruction and inverse crime
- implementation and analysis of the parameters' impact on the reconstruction

Limits

- naive and primitive work for a domain > 100 years old
- made simplified hypotheses (linear interpolation, CT reconstruction method *per se*) to get an easier formulation

Perspectives

- theoretical convergence analysis of the discretization parameters
- non-uniform densities (didn't see those ideas in my literature review)
- irregular discretization to enhance particular structures?
- extract knowledge from our "elliptical Fourier slice Theorem" to design a better reconstruction algorithm for ellipses only?
- towards a new Shannon "sinogram sampling" theorem?

-  Abergel, Rémy and Lionel Moisan (2017). *The Shannon Total Variation*.
-  Bauer, Daniel, Humberto Chaves, and C. Arcoumanis (2012). *Measurements of void fraction distribution in cavitating pipe flow using x-ray CT*.
-  Brown, Robert et al. (2014). *Magnetic Resonance Imaging: Physical Principles and Sequence Design: Second Edition*.
-  Guerquin-Kern, Matthieu et al. (2012). *Realistic Analytical Phantoms for Parallel Magnetic Resonance Imaging*.
-  Herman, Gabor T. (2009). *Fundamentals of Computerized Tomography: Image Reconstruction from Projections*.
-  Kak, A.C. and M. Slaney (2001). *Principles of Computerized Tomographic Imaging*.
-  Koay, Cheng Guan, Joelle E. Sarlls, and Evren Özarslan (2007). *Three-dimensional analytical magnetic resonance imaging phantom in the Fourier domain*.
-  Lysaker, Marius, Arvid Lundervold, and Xue-Cheng Tai (2003). *Noise removal using fourth-order partial differential equation with applications to medical magnetic resonance images in space and time*.

-  Pruessmann, Klaas P. et al. (1999). *SENSE: Sensitivity encoding for fast MRI.*
-  Ripoll, Olivier, Ville Kettunen, and Hans Herzig (2002). *Low-data simulation of diffractive optical elements based on the zones geometry.*
-  Rudin, Leonid I., Stanley Osher, and Emad Fatemi (1992). *Nonlinear total variation based noise removal algorithms.*
-  Shepp, LA et al. (1980). *Computerized tomography and nuclear magnetic resonance.*
-  Shepp, Larry A. and Benjamin F. Logan (1974). *The Fourier reconstruction of a head section.*

Thank you for your attention